

pubs.acs.org/JPCB Article

Multiscale Simulation of Protein Corona Formation on Silver Nanoparticles: Study of Ovispirin-1 Peptide Adsorption

Pranab Sarker, Md Symon Jahan Sajib, Xiuping Tao, and Tao Wei*



Cite This: J. Phys. Chem. B 2022, 126, 601-608



ACCESS I

III Metrics & More

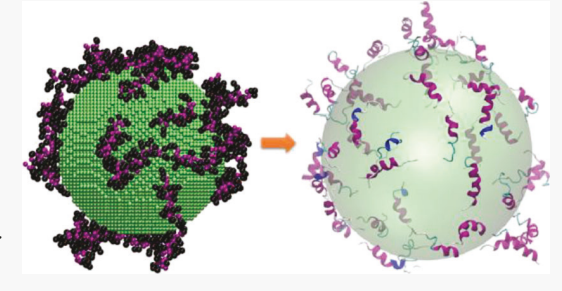


Article Recommendations



Supporting Information

ABSTRACT: The exposure of nanoparticles (NPs) to biofluids leads to the rapid coverage of proteins, named protein corona, which alters the NPs' chemicophysical and biological properties. Fundamental studies of the protein corona are thus critical to the increasing applications of NPs in nanotechnology and nanomedicines. The present work utilizes multiscale simulations of a model biological system, small ovispirin-1 peptides, and bare silver nanoparticles (AgNPs) to examine the NPs' size and surface hydrophilicity effects on formation dynamics and the structure of the peptide corona. Our simulations revealed the different adsorption dynamics of ovispirin-1 peptides on the NPs, including the direct adsorption of a single peptide and peptide aggregates and multistep adsorption, as well as an



intermediate cycle of desorption and readsorption. Notably, the whole process of peptide adsorption on hydrophilic AgNP surfaces can be generalized as three stages: diffusion to the surface, initial landing via hydrophilic residues, and the final attachment. The decrease in AgNP's size leads to faster adsorption with more heterogeneous peptide interfacial dynamics, a denser and inhomogeneous peptide packing structure, and a wider distribution of adsorption orientations. Subsequent atomistic molecular dynamics simulations demonstrated that on the hydrophilic AgNP surfaces, adsorbed peptides display moderate changes in their secondary structure, resulting in further changes of corona composition, i.e., amino acid residue distribution on the surface.

INTRODUCTION

The interactions of engineered metal nanoparticles (NPs) with proteins and peptides have gained increasing attention due to their broad range of applications in nanotechnology. 1-7 Owing to their unique electronic and optical properties, high surfaceto-volume ratio, ease in synthesis, and antibacterial effect, silver nanoparticles (AgNPs) are being widely used for drug delivery, sensors, textile fabrics, and wood flooring. The exposure of NPs to biological fluids leads to protein adsorption and the formation of a protein corona, 10 which alters chemicophysical and biological properties of NPs' surfaces and may also trigger biological responses. 11 Therefore, it is imperative to study the interaction between AgNPs and the protein corona formation process and the post corona

General experimental methods, such as Fourier transform infrared spectroscopy (FTIR), surface plasmon resonance (SPR), and circular dichroism (CD), elucidate ensembleaveraged measurement of the protein structure and interfacial dynamics at the solid-liquid interface. 13-15 Significant experimental efforts 13,14 were made to understand the interactions between a AgNP and different proteins due to their increasing mass production and broad applications. 2-6,8,9 For example, using linear optical spectroscopies, Podila et al. demonstrated that the structural denaturation of proteins leads to the formation of a protein corona on uncoated and surfactant-free AgNPs. 13 A study using surface-enhanced

Raman scattering (SERS) and CD spectroscopies by Treuel et al. showed that polymer coatings of AgNPs could prevent sulfur-Ag bonding and greatly reduce bovine serum albumin (BSA) proteins' binding affinity. 14 In another work, Ashkarran et al. investigated the structural (cube, sphere, wire, and triangle) effect of AgNPs on the protein corona formation with fetal bovine serum. 16 Their work reveals that the concentration and composition of the corona are highly morphologydependent due to both the curvature effect and coordination of the surface atoms, which facilitate different surface energies and hence the difference in protein binding. 16 Using mass spectrometry proteomics, researchers also studied the AgNP surface charge effect and showed that there is a twofold decrease in the anionic proteins bound to negative citratecoated 10 and 100 nm AgNPs, compared to positive branched polyethyleneimine-coated ones. 12

Despite considerable previous efforts, fundamental studies at the molecular level are still highly desired. The corona formation comprises many molecular subprocesses, such as

Received: September 19, 2021 January 3, 2022 Revised: Published: January 14, 2022





adsorption, desorption, diffusion, conformational change, and aggregation. As such, the corona buildup itself is a complex process, and a comprehensive understanding of it requires grasping of all microscopic subprocesses, short-lived or long-lived. However, it is currently impossible to comprehend the molecular/atomistic level details of protein corona structures or compositions with general experiments. Also, it is challenging to study in experiments the soft corona that comprises short-lived loosely bound proteins. These proteins usually get washed away during the separation process of the corona from the incubation medium through subsequent centrifugation and washing steps. 18

To complement experimental measurements, molecular dynamics (MD) simulations at both atomistic and coarsegrained levels are being used as a powerful tool to study the adsorption behavior of proteins and peptides in explicit water at the microscopic scale. 19-33 Atomistic MD simulations can identify structural changes of biomolecules with high resolutions up to the atomistic scale. 19,29,34 Coarse-grained molecular dynamics (CGMD) simulations, which present a molecule with simplified coarse-grained beads, are more efficient than atomistic MD simulations to model a system, involving a large number of lipids, biomolecules, water, and other components in the solution, at the mesoscopic level. 29,31,35 Ramezani and Rafii-Tabar performed atomistic MD simulations to study the unfolding process of serum albumin on the AuNP surface and determine the key amino acids that drive their interactions.³⁴ Yu and Zhou performed CGMD simulations to show that with the increase of silica NP size, the adsorbed lysozyme protein has a narrower orientation distribution.³¹ Hybrid multiscale CGMD and atomistic MD simulations, which can achieve both computational efficiency and atomistic/molecular resolution, were also performed to study the protein corona on NPs. 29,32,33 Sajib et al. carried out hybrid CGMD/atomistic simulations and showed that the corona structure depends on both protein's type and NPs' size, e.g., a homogeneous single-layered structure for ovispirin-1 peptides and the inhomogeneous multilayered aggregates for lysozyme proteins on gold NP (AuNP) surfaces.²⁹ Another simulation study from Käkinen et al. illustrated that the conformational change of luciferase proteins is mainly introduced by the electrostatic interactions between anionic luciferase residues and cationic citrate-coated AgNP surfaces.³² Tavakol and co-workers studied the fibrinogen protein corona on polystyrene NPs and showed that the presence of metabolomes (glucose and cholesterol) changed the binding site of the protein and affected the amounts of proteins and the structure of the protein corona on NPs.33

In this study, hybrid CGMD and atomistic MD simulations were performed to study the protein corona formation on AgNP surfaces. We focused on the effects of NP surface's hydrophilicity and size or curvature, as they are key factors for the protein corona formation dynamics and structure. To isolate other effects, such as morphologies, charges, rigidity, roughness, and strong thiol—metal surface interactions, which also govern the protein corona formation, we chose an ideal model system of bare hydrophilic AgNPs. ^{36–38} Our modeled AgNPs are free from oxidation, contamination, ligand-treatment, and strong sulfur—Ag binding, as the small-sized antimicrobial peptide ovispirin-1³⁹ has no cysteine amino residue. Our multiscale simulations offered a more complete understanding of the interfacial behaviors of peptides on the hydrophilic NPs' surfaces. Our fundamental studies of the

protein corona on AgNPs will be critical to future applications of NPs in nanomedicines and other nanotechnologies.

METHODS

CGMD Simulations. CGMD simulations were performed using the Martini 3.0 force field⁴⁰ and the GROMACS⁴¹ software package (version 2019.6). In the Martini framework, an elastic network connecting the CG beads is imposed to constrain the protein secondary structure. The conversion of these beads from the initial all-atoms structure was accomplished with the martinize.py script.40 The initial allatom models of ovispirin-1 were obtained from the protein data bank (pdb code: 1HU5). With periodic boundary conditions (PBC), the NVT ensembles of the Martini-beads were incorporated for all CGMD simulations. The nonbonded neighbors' list was updated every 20 steps, using the Verlet cutoff scheme. The temperature of the peptides, NPs, water, and ions was controlled separately using a velocity-rescale thermostat at 300 K. A time step of 20 fs was chosen to integrate the equation of beads' motion.

A converted ovispirin-1 model includes 47 CG beads with a net charge of +7. The Martini forcefield incorporates both bonded interactions and nonbonded interactions between beads. The nonbonded interactions include both Lennard-Jones (LJ) and electrostatic potentials. The LJ interaction is defined as,

$$U_{\mathrm{LJ}}(r_{ij}) = 4\varepsilon_{ij} \left[\left(\frac{\sigma_{ij}}{r_{ij}} \right)^{12} - \left(\frac{\sigma_{ij}}{r_{ij}} \right)^{6} \right] \tag{1}$$

where r_{ij} , σ_{ij} , and ε_{ij} stand for the distance, the effective bead size, and the strength of the interaction between two beads i and j, respectively. Based on the type of beads, ε_{ij} is within the range of 2.0–5.6 kJ/mol. $\sigma_{ij}=0.62$ nm was set for the charged or apolar beads while 0.47 nm for others. Following the previous studies in the literature, ⁴² AgNPs with diameters of 3.2 and 10 nm were modeled with an atomistic structure, directly cut from the silver crystal lattice. To model bare AgNP surfaces of hydrophilic nature, ^{36–38} each atom of AgNP was assigned with Martini P4-type hydrophilic CG beads by following the previous study in the literature. ⁴³ The choice of the hydrophilic nature for the bare AgNPs is consistent with the experiment ^{36–38} and previous simulation. ⁴³ The interactions between the CG beads of AgNPs with water and peptides were represented by $\sigma=0.47$ nm, $\varepsilon=4.55\frac{kJ}{mol}$. The electrostatic potential of protein-charged beads are represented as,

$$U_{\rm ele}(r_{ij}) = \frac{q_i q_j}{4\pi\epsilon_0 \epsilon_r r_{ij}} \tag{2}$$

where q_i and q_j are the charges of beads i and j, respectively; ϵ_0 is the vacuum permittivity; and ϵ_r is the relative permittivity. The electrostatic interactions are imposed with a cutoff distance of 1.1 nm.

For the initial configuration of CGMD, both 3.2 and 10 nm AgNPs were assembled with 44 ovispirin-1 peptides in cubic boxes with the sizes of $26 \times 26 \times 26$ and $26.25 \times 26.25 \times 26.25$ nm³, respectively, to maintain the same mass concentration of peptide in both cases. Simulation boxes were solvated with coarse-grained beads of the Martini

standard water model, and counterions were added to neutralize the systems.

Atomistic MD Simulations. Since the CG simulations with the Martini force field parameters 7,40 constrain the protein secondary structure, we employed all-atom MD simulation to investigate the structural changes of the adsorbed ovispirin-1 peptides on the 10 nm AgNP surfaces. The final configuration of the protein corona on a 10 nm AgNP was obtained from CG simulation to this end, and the reverse mapping protocol was utilized to obtain the all-atom structure, which was later used as the initial configuration of the atomistic MD simulation. The peptides were re-solvated using the atomistic water model of TIP3P and neutralized with counterions. CHARMM36 forcefield parameters⁴⁴ were adopted to model peptide's bonded and nonbonded interactions. The Ag-peptide and Ag-water atomistic interactions were modeled with LJ potentials obtained from the literature.45

To minimize the computational load, a smaller box of $15.94 \times 15.94 \times 15.94 \times m^3$ was chosen for the atomistic simulations. The system was equilibrated with NPT at 1 bar for 200 ns, using the Parrinello–Rahman method, after a short equilibration step in the NVT ensemble at 298.15 K. The simulations in NPT can achieve the accuracy in water density of the system.

In the NVT step, the thermostat method of the velocity rescale was employed by keeping all peptides constrained. For the NPT production run, a time step of 1.0 fs with the leapfrog algorithm was incorporated to integrate the dynamics. For the long-range electrostatic interactions, the Particle Mesh Ewald summation with a cutoff distance of 1.2 nm for separating the direct and reciprocal space was used. The cutoff for LJ potential was set as 1.2 nm, while the long-range dispersion effect on energy and pressure was applied.

RESULTS

Dynamics of Ovispirin-1 Corona Formation. The final ovispirin-corona structures for two differently sized NPs (3.2 and 10 nm) obtained from the CGMD simulations are displayed in Figure 1. As expected, the larger AgNP with more

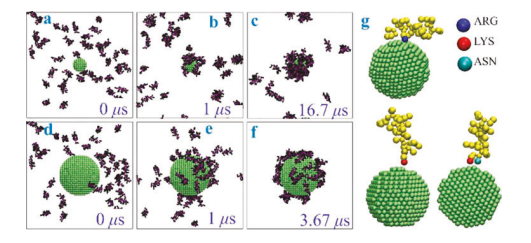


Figure 1. Corona formation dynamics for (a-c) 3.2 nm and (d-f) 10 nm AgNPs. (g) Peptides' preferable landing sites (ARG4,5,8, LYS1,15,16, and LYS1-ASN2) while adsorbing on the 3.2 nm AgNP surface.

available surface area exhibits faster adsorption of ovispirins. All 44 ovispirins are adsorbed on the 10 nm NP surface by 3.67 μs (Figure 1d–f), while 13 peptides remain in the bulk even up to $\sim 16.7~\mu s$ (Figure 1a–c) on the 3.2 nm NP surface due to the unavailability of enough surface area for adsorption. Tracing of all the peptides' initial landings on both hydrophilic AgNP surfaces shows that the ovispirins adsorb primarily with hydrophilic residues of LYS1,15,16 and ARG4,5,8 (see Figure 1g for the 3.2 nm NP and Figure S1 in the Supporting Information for the 10 nm NP). Landing through the residues

of ARG4,5,8, peptides prefer to lie down on (tangential to) the surface to adopt the side-on landing (Figure 1g). In contrast, an end-on landing with the upright (normal to the surface) orientation residues is more prevalent, when the landing residues are LYS1,15,16 (Figure 1g). A rare case of stand-up landing through ASN2, which is next to LYS1, was also observed on the surface of 3.2 nm NP (Figure 1g (downright)).

Counterintuitively, our study here shows that the initial landing of the peptide on a hydrophilic NP is not kineticcontrolled and can be well correlated with hydrophilicity of the NP surface and amino acid residues. As shown in our previous studies, protein adsorption and orientation are not solely protein-surface interaction-driven.²² Hydration and dehydration of surfaces of the substrate and the protein also play a key role in the short range at a distance of about one-layer water thickness, which can be presented as $\gamma \Delta A$ (γ stands for surface tension and ΔA for surface area).²² The total ΔA for the protein-surface complex decreases upon protein adsorption and $\gamma \Delta A$ becomes a driving force. However, the interfacial water must be depleted for peptides to land on the surface, which exhibits an energy barrier for the biomolecule's initial landing on the surface. ^{19,22} The initial landing is mainly driven by the protein-surface interactions as well as the Brownian thermal motion, since most part of a peptide is beyond the range of the short-range interaction of $\gamma \Delta A$. This explains the observation of our simulations here about the correlation of hydrophobicity of the landing sites of peptides and the surface for both small and large NPs. After the initial landing, as a peptide is closer to the surface, the final anchoring is governed by both $\gamma \Delta A$ and peptide-surface interactions. For a larger AgNP of 10 nm (with a smaller curvature), compared to a smaller NP of 3.2 nm (with a larger curvature), due to a larger available surface area ΔA , the energy term $\gamma \Delta A$ becomes stronger, which results in faster adsorption, larger degree of reorientation peptides and the final side-on anchoring, which will be demonstrated in the following discussion. It is worth noting that due to the computational load, we cannot simulate a large number of peptides in explicit water in order to maintain the peptide bulk concentration as a constant to study the adsorption process at the steady state. Our current work only focused on the initial adsorption of peptides, which are adjacent to the NP's surface, as we expect no significant difference in the adsorption kinetics of our system compared to that in a system with a large number of peptides. The reason is that peptides in the bulk water far away from the NPs spend a long time in diffusion, since they are not affected by the peptide-surface interactions and the short-range driving force of $\gamma \Delta A$.

In our simulations, the radial distribution function g(r) of water shows a condensed hydration layer shell surrounding hydrophilic AgNP surfaces (Figure S3 in the Supporting Information). Figure 2a–f gives two examples to illustrate the entire microscopic dynamic process, which consists of diffusion in the bulk, the initial landing (the side-on and the end-on), and subsequent adsorption. Initially, the ovispirin-1 peptide diffuses from the bulk water toward the NPs and then it penetrates the NP surface's hydration shell to land on the hydrophilic AgNP surfaces through the hydrophilic residues of ASN2 and LYS1 (Figure 2b). Similar observations of peptide landing on the surface via its strongest binding site(s) to overcome the energy barrier of the interfacial hydration were also reported in previous MD simulations.

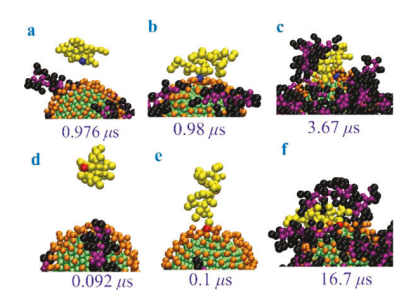


Figure 2. Dynamics of peptide's initial landing and the subsequent adsorption on the surface of the 3.2 nm AgNP for both cases of the initial side-on landing (a-c) and end-on landing (d-f). Hydration water molecules within the first hydration shell of AgNP surfaces are colored orange; the landing residue of ARG is colored blue and LYS is red; the backbone of peptides is black; and the sidechains are purple.

of initial landing sites (not to the entire production run) for the 3.2 nm AgNP are: LYS1 (58%), LYS9 (5%), LYS15 (11%), LYS16 (5%), ARG8 (15.8%), and ASN2 (5.2%) and for the 10 nm AgNP are: LYS1 (46%), LYS16 (23%), ARG4 (15.4%), and ARG5 (15.4%).

Subsequently, the ovispirin-1 peptide approaches closer to the NP surface while undergoing a certain degree of rotation, particularly in the initial end-on landing for the case of 10 nm AgNP, to achieve maximum contact with the surface under the effect of the large silver—water surface tension γ (1.12–1.25 J/ m²).⁴⁵ The final orientation of the peptide is also affected by the local peptide-peptide interactions on the NP surface (Figure 2) due to the crowding effect. As shown in our previous analyses of protein binding free energy, 22,23 on an uncharged surface, one of the dominant effects on protein adsorption is due to the metal surface's large metal-water surface tension when the protein is adjacent to the surface. The three-stage peptide adsorption mechanism (bulk diffusion; initial landing; and final adsorption) on AgNPs observed in our CGMD simulations is consistent with the findings of previous studies 19,46 of peptide/protein adsorption on hydrophobic and hydrophilic surfaces using atomistic MD simulations.

Multiple adsorption modes are observed in our simulations irrespective of their sizes and curvature, which are accomplished either in one or multisteps. The primary mode of adsorption is one-step, wherein a single ovispirin-1 peptide (Figure 3a for the 3.2 nm AgNP and Figure S2a for the 10 nm AgNP in the Supporting Information) or peptide aggregate in

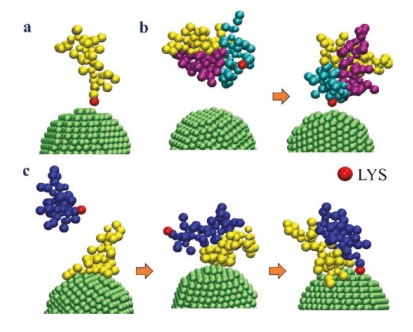


Figure 3. Adsorption mechanisms on a 3.2 nm AgNP surface. Onestep adsorption in which a single (a) or a cluster of peptides aggregated in bulk lands directly on the surface (b). (c) Two-step adsorption: a single peptide attaches itself to another peptide adsorbed on the surface at first, followed by rotation and landing on the surface.

bulk (Figure 3b for the 3.2 nm AgNP and Figure S2b for the 10 nm AgNP in the Supporting Information) directly attaches itself to the NP surface. Peptides also can adsorb on the surface through the multistep mode. In the latter case, an ovispirin-1 peptide initially lands on an already adsorbed peptide, subsequently rolling over it to achieve direct contact with the surface (Figure 3c for the 3.2 nm AgNP and Figure S2c for the 10 nm AgNP in the Supporting Information). Heterogeneous peptide adsorption kinetics were also detected in previous experimental studies of single-molecule total internal reflection fluorescence microscopy 47,48 and mesoscopic simulations using Langevin dynamics.

Tracking the ovispirins further reveals that peptides adsorbed through the multistep mechanism can desorb and readsorb, as shown in Figure 3c. Given our simulation time of microseconds, peptides, which adsorbed directly on the surface via the one-step mode (Figures 3a,b and S2 in the Supporting Information), do not desorb. However, the peptide (blue beads in Figure 3c) that aggregates with a preadsorbed peptide (yellow beads in Figure 3c) can undergo the desorption—readsorption cycle. This cycle of intermediate states is in fact a notable feature of protein adsorption on the 3.2 nm NP (Figure 4a—d). In contrast, in the case of the 10 nm AgNP,

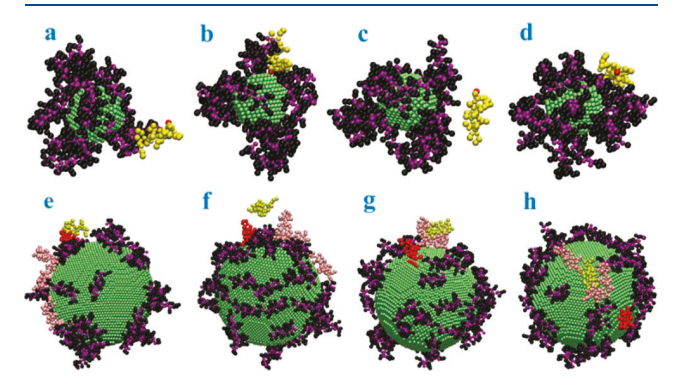


Figure 4. Peptide's adsorption—desorption—readsorption cycle. A protein with yellow beads (a) adsorbs on a protein aggregate in the first place followed by its brief attachment to the 3.2 nm AgNP surface (b). This peptide desorbs (c) and eventually readsorbs (d) on another peptide. (e—h) Similar pattern of a peptide's (yellow beads) adsorption—desorption—readsorption on the 10 nm surface except for its attachment to the surface in the end.

only a single peptide participates in such a process in our simulations (Figure 4e–h). Although these rare events in our CG MD simulations are in the time scale of microseconds, they bear significant importance in the larger time and macroscopic scale involving many NPs.⁴⁷

The events of peptides' adsorption—desorption—readsorption detected in our CGMD simulations are due to the Brownian thermal motion in the aqueous environment, the lack of surface area available for landing on the 3.2 nm AgNP, and the weak surface—peptide and peptide—peptide attractions. It is also notable that in our simulations, the phenomena of desorption of preadsorbed peptides due to the collision of bulk peptides were not detected. As shown in Figure 4 as an example, in the case of the 3.2 nm AgNP, one of the peptides desorbs even after landing on the surface. As such, its attachment on the surface is not stable, resulting in desorption. As a result, the cycle of adsorption—desorption—readsorption of peptides is a hallmark of the 3.2 nm AgNP—peptide

interactions. In contrast, such an adsorption—desorption—readsorption event is barely detected for the 10 nm AgNP (Figure 4e—h). Given the sufficient surface area for landing simultaneously, most of the peptides can directly contact the surface and maximize their interactions with it. These landed peptides are thus not seen to be desorbed. As shown in Figure 4e,f, the sole peptide (yellow beads) that lands on an adsorbed peptide keeps diffusing on other two peptides (pink beads) before rolling over and getting adsorbed on the surface, after which it does not desorb. Such an event suggests that a single peptide's propensity to attach to the surface varies with curvature (or NP size), and this tendency increases with the larger surface.

Structure of the Ovispirin-1 Corona. Next, we examined the packing structures of coronas. Figure 5 shows an analysis of

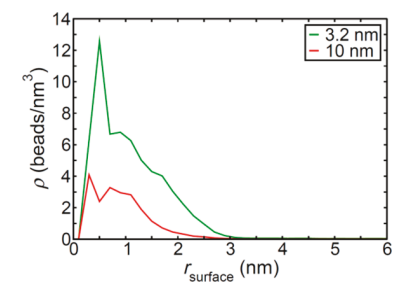


Figure 5. Peptides' CG particle beads' density ρ as a function of the distance to the AgNP surface ($r_{\text{surface}} = r - r_{ii}$, $r_i = 1.6$ or 5 nm is the AgNP radius).

the distribution of adsorbed peptides on the NP surfaces by monitoring CG beads' radial density. In consistence with Figure 1a–f, the ovisprin corona on the 3.2 nm NP has a larger surface density than that of the 10 nm AgNP, due to the less available surface area where ovispirins are more compactly adsorbed. On the small 3.2 nm AgNP, peptides form an inhomogeneous multilayer aggregate. Such stacking and aggregating structure of multiple peptides was not significant on the surface of the large 10 nm AgNP in which all proteins were adsorbed on the surface.

To further understand the size effect of NPs on the peptide corona structure, we quantified the orientations of the adsorbed peptides, as illustrated in Figure 6. A radial vector

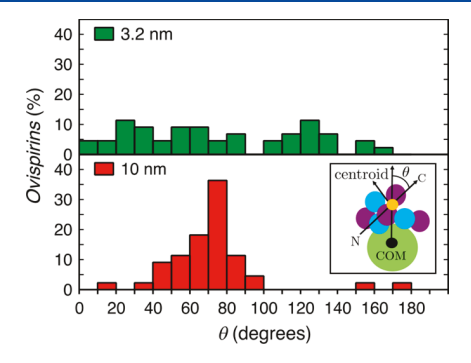


Figure 6. Orientation distribution of ovispirin-1 peptides on the AgNP surfaces simulated in CGMD. Shown in the inset are the chosen two vectors between which the angle (θ) is calculated. One directs from the center-of-mass (COM) of the AgNPs to the centroid of the protein beads and the other does from the N-terminus to the C-terminus of the corresponding peptide. For the complete standing-up, $\theta=0$ or 180° and for the lying-down, $\theta=90^\circ$.

and a peptide's terminus connecting vector are used to calculate the angles, and both of these go through the centroid of the peptide (see the inset in Figure 6). The former connects the COM of the AgNPs and the centroid, whereas the latter also goes through the centroid but directly from the Nterminus to the C-terminus. The centroid is determined by the singular value decomposition of peptide beads' positions in three dimensions. While $\theta = 90^{\circ}$ corresponds to complete lying-down adsorption of an ovispirin-1 peptide on the surface, it is 0 or 180° when an ovispirin-1 peptide has a totally standup adsorption. As shown in Figure 6, peptides have an orientation preference of lying-down on the 10 nm AgNP surface, consistent with the observation in the case of a flat surface. 50 However, on the surface of the small AgNP (3.2 nm), the adsorbed ovispirin-1 peptides have a wide distribution of the orientations. Another observation is that the orientation preference of peptides on the NPs is not as strong when the surface becomes more hydrophilic. In our previous CGMD simulations²⁹ of ovispirin-1 adsorption on AuNP surfaces, which was modeled to be hydrophobic, peptides are more likely to stand up on the AuNP surfaces compared with hydrophilic AgNP surfaces in this study.

The number $N_{\rm ads}$ of adsorbed residues at a given cutoff of the radius (3.1 Å from the 10 nm AgNP surface obtained from the peak position in Figure 5) was monitored for the 10 nm AgNP using the final configurations of the CGMD and atomistic MD simulations. As Figure 7 shows, in the CGMD

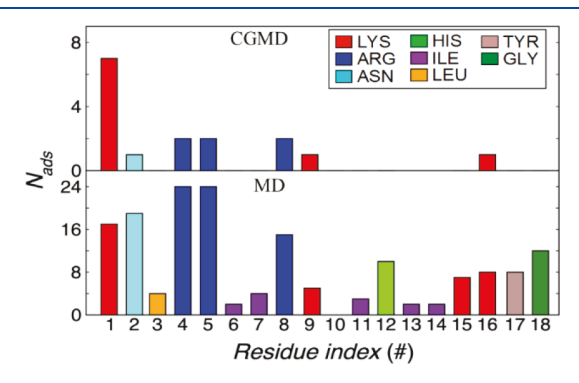


Figure 7. Distribution of adsorbed residues on the 10 nm AgNP surface. $N_{\rm ads}$ is the total number of adsorbed residues on the surface within a cutoff distance of 3.1 Å from the 10 nm AgNP surface.

simulations where the peptide structure was constrained, hydrophilic residues (LYS, ARG, and ASN) are in direct contact with the hydrophilic AgNP surfaces. However, when the same distribution of beads is reversely mapped to all-atom residues and relaxed for another 230 ns atomistic MD simulation to take into account the changes in the peptide's secondary structures, the distribution of residues on the AgNP surface changes. Compared to the CGMD simulations, the subsequent atomistic MD showed that the hydrophilic majority of LYS, ARG, and ASN still holds but drops to ~60%, whereas the percentages of LEU and ILE increase. The difference in the surface residues' compositions for the configurations obtained with CG and atomistic MD simulation is mainly due to the alternation of peptides' secondary structure, which will be discussed in the following section.

Secondary Structure of the Adsorbed Ovispirin-1 Peptides. We further analyze the secondary structural component distribution in the corona structure of the 10 nm AgNP to understand the structural changes of the adsorbed peptides. Obtained from the all-atom MD simulation of 230 ns, as shown in Figure 8, the secondary structures of peptides

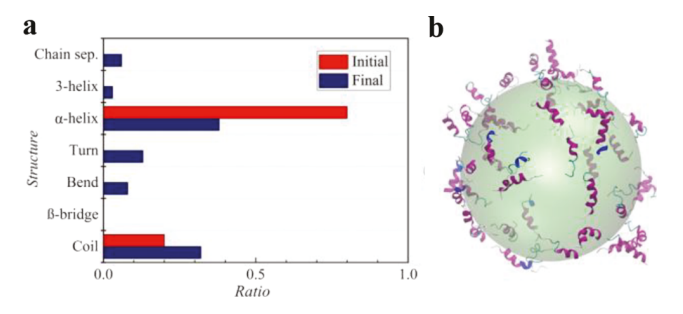


Figure 8. (a) Averaged secondary structure of adsorbed peptides on the 10 nm AgNP surface in comparison with the peptide's crystal structure and (b) snapshot of the final configuration of peptides on the AgNP surfaces.

were analyzed using DSSP (database of secondary structure assignments). Compared with the ovispirin-1 peptide in bulk water, the adsorbed peptides exhibit a structural change (Figure 8a). In bulk water, ovispirin-1 has two secondary structure types: α -helix (82%) and coil (18%), whereas the adsorbed peptides also have 41% α -helix and 32% coil, including additional four secondary structure types—chain separator, 3-helix, turn, and bend. Due to the 50% loss of its initial α -helix, the adsorbed protein gained variations in its secondary structure. As expected, the changes of secondary structures of the adsorbed peptides introduce further alteration of the corona composition, i.e., amino acid residue distribution on the surface as evidenced in Figure 7.

DISCUSSION AND CONCLUSIONS

The formation of the protein corona on NPs affects their surface properties and applications. Fundamental studies using computer simulations in this perspective at the molecular level, which can complement general experimental studies, are critical to widen NP applications and are essential for theoretical modeling development. We performed multiscale simulations to provide insight into the protein corona formation dynamics and peptides' structural changes using the model systems of bare hydrophilic AgNPs and small ovispirin-1 peptides.

Different microscopic kinetics of peptide adsorption on NPs were detected in the mesoscopic CGMD simulations, including the one-step adsorption of a single peptide and peptide aggregates and multistep adsorption. Analyses of multiple trajectories of the adsorbed peptides simulated in our mesoscopic CGMD simulations demonstrated that the entire process of peptide adsorption on the hydrophilic AgNP surfaces consists of three stages. More specifically, the ovispirin-1 peptides initially land on AgNP surfaces via their several hydrophilic residues to overcome the energy barrier of the interfacial hydration shell on AgNP surfaces, following the initial diffusion from the bulk water. Subsequently, the peptides achieve more contact with the NPs' surfaces governed by the large silver-water surface tension and interactions with preadsorbed peptides on the NP surfaces. Our atomistic MD simulations also revealed that the structural denaturing of the adsorbed peptides introduces further changes in the corona composition, i.e., amino acid residue distribution on the

surface. As the size of NPs decreases, which indicates the increase of the curvature, peptides can undergo more motions of adsorption—desorption—readsorption. The packing density on a smaller NP is higher than that of the large AgNP. Peptides have a wider orientational distribution on a small NP than on a large one.

ASSOCIATED CONTENT

Supporting Information

The Supporting Information is available free of charge at https://pubs.acs.org/doi/10.1021/acs.jpcb.1c08267.

Figures of peptides' preferrable landing sites on the 10 nm AgNP surface, adsorption mechanisms on the 10 nm AgNP surface, and the radial distribution function of water coarse-grained beads for the 3.2 nm AgNP surface (PDF)

AUTHOR INFORMATION

Corresponding Authors

Xiuping Tao — Department of Chemistry, Winston-Salem State University, Winston-Salem, North Carolina 27110, United States; Email: taoxi@wssu.edu

Tao Wei — Department of Chemical Engineering, Howard University, Washington, D.C. 20059, United States; orcid.org/0000-0001-6888-1658; Email: tao.wei@howard.edu

Authors

Pranab Sarker — Department of Chemical Engineering, Howard University, Washington, D.C. 20059, United States Md Symon Jahan Sajib — Department of Chemical Engineering, Howard University, Washington, D.C. 20059, United States

Complete contact information is available at: https://pubs.acs.org/10.1021/acs.jpcb.1c08267

Author Contributions

[†]P.S. and M.S.J.S. contributed equally.

Notes

The authors declare no competing financial interest.

ACKNOWLEDGMENTS

T.W. and X.T. thank the grant support from the National Science Foundation (NSF 1831559 to T.W. and 1831548 to X.T.). T.W. is indebted to grant support of the ESD HBCU/MI solicitation (OPO300-RTB.34.HBCU.21.01.RSA) from NASA/JPL and computational resources from the program of the Extreme Science and Engineering Discovery Environment (XSEDE) and the Texas Advanced Computing Center (TACC).

■ REFERENCES

- (1) Petryayeva, E.; Krull, U. J. Localized surface plasmon resonance: Nanostructures, bioassays and biosensing—A review. *Anal. Chim. Acta* **2011**, *706*, 8–24.
- (2) Zhou, H.; Yang, D.; Ivleva, N. P.; Mircescu, N. E.; Niessner, R.; Haisch, C. SERS detection of bacteria in water by in situ coating with Ag nanoparticles. *Anal. Chem.* **2014**, *86*, 1525–1533.
- (3) Cañamares, M. V.; Garcia-Ramos, J.; Domingo, C.; Sanchez-Cortes, S. Surface-enhanced Raman scattering study of the adsorption of the anthraquinone pigment alizarin on Ag nanoparticles. *J. Raman Spectrosc.* **2004**, *35*, 921–927.

- (4) Zhu, Y.-X.; Jia, H.-R.; Pan, G.-Y.; Ulrich, N. W.; Chen, Z.; Wu, F.-G. Development of a light-controlled nanoplatform for direct nuclear delivery of molecular and nanoscale materials. *J. Am. Chem. Soc.* **2018**, *140*, 4062–4070.
- (5) Ravindra, S.; Murali Mohan, Y.; Narayana Reddy, N.; Mohana Raju, K. Fabrication of antibacterial cotton fibres loaded with silver nanoparticles via "Green Approach". *Colloids Surf. A Physicochem. Eng. Asp.* **2010**, *367*, 31–40.
- (6) Kim, S.; Kim, H.-J. Anti-bacterial performance of colloidal silver-treated laminate wood flooring. *Int. Biodeterior. Biodegrad.* **2006**, *57*, 155–162.
- (7) Ghosh, S. K.; Kundu, S.; Mandal, M.; Pal, T. Silver and gold nanocluster catalyzed reduction of methylene blue by arsine in a micellar medium. *Langmuir* **2002**, *18*, 8756–8760.
- (8) Peer, D.; Karp, J. M.; Hong, S.; Farokhzad, O. C.; Margalit, R.; Langer, R. Nanocarriers as an emerging platform for cancer therapy. *Nat. Nanotechnol.* **2007**, *2*, 751–760.
- (9) Bamrungsap, S.; Zhao, Z.; Chen, T.; Wang, L.; Li, C.; Fu, T.; Tan, W. Nanotechnology in therapeutics: a focus on nanoparticles as a drug delivery system. *Nanomedicine* **2012**, *7*, 1253–1271.
- (10) Durán, N.; Silveira, C. P.; Durán, M.; Martinez, D. S. T. Silver nanoparticle protein corona and toxicity: a mini-review. *J. Nanobiotechnol.* **2015**, *13*, 55.
- (11) Jiang, S.; Cao, Z. Ultralow-fouling, functionalizable, and hydrolyzable zwitterionic materials and their derivatives for biological applications. *Adv. Mater.* **2010**, *22*, 920–932.
- (12) Eigenheer, R.; Castellanos, E. R.; Nakamoto, M. Y.; Gerner, K. T.; Lampe, A. M.; Wheeler, K. E. Silver nanoparticle protein corona composition compared across engineered particle properties and environmentally relevant reaction conditions. *Environ. Sci.: Nano* **2014**, *1*, 238–247.
- (13) Podila, R.; Chen, R.; Ke, P. C.; Brown, J. M.; Rao, A. M. Effects of surface functional groups on the formation of nanoparticle-protein corona. *Appl. Phys. Lett.* **2012**, *101*, 263701.
- (14) Treuel, L.; Malissek, M.; Grass, S.; Diendorf, J.; Mahl, D.; Meyer-Zaika, W.; Epple, M. Quantifying the influence of polymer coatings on the serum albumin corona formation around silver and gold nanoparticles. *J. Nanopart. Res.* **2012**, *14*, 1102.
- (15) Wei, T.; Kaewtathip, S.; Shing, K. Buffer effect on protein adsorption at liquid/solid interface. *J. Phys. Chem. C* **2009**, *113*, 2053–2062.
- (16) Ashkarran, A. A.; Ghavami, M.; Aghaverdi, H.; Stroeve, P.; Mahmoudi, M. Bacterial effects and protein corona evaluations: crucial ignored factors in the prediction of bio-efficacy of various forms of silver nanoparticles. *Chem. Res. Toxicol.* **2012**, 25, 1231–1242.
- (17) Kastantin, M.; Langdon, B. B.; Schwartz, D. K. A bottom-up approach to understanding protein layer formation at solid—liquid interfaces. *Adv. Colloid Interface Sci.* **2014**, 207, 240—252.
- (18) Miclăuş, T.; Bochenkov, V. E.; Ogaki, R.; Howard, K. A.; Sutherland, D. S. Spatial mapping and quantification of soft and hard protein coronas at silver nanocubes. *Nano Lett.* **2014**, *14*, 2086–2093.
- (19) Wei, T.; Carignano, M. A.; Szleifer, I. Lysozyme adsorption on polyethylene surfaces: why are long simulations needed? *Langmuir* **2011**, 27, 12074–12081.
- (20) Wei, T.; Carignano, M. A.; Szleifer, I. Molecular dynamics simulation of lysozyme adsorption/desorption on hydrophobic surfaces. *J. Phys. Chem. B* **2012**, *116*, 10189–10194.
- (21) Wei, T.; Sajib, M. S. J.; Samieegohar, M.; Ma, H.; Shing, K. Self-Assembled Monolayers of an Azobenzene Derivative on Silica and Their Interactions with Lysozyme. *Langmuir* **2015**, *31*, 13543–13552.
- (22) Nakano, C. M.; Ma, H.; Wei, T. Study of lysozyme mobility and binding free energy during adsorption on a graphene surface. *Appl. Phys. Lett.* **2015**, *106*, 153701.
- (23) Zhang, T.; Wei, T.; Han, Y.; Ma, H.; Samieegohar, M.; Chen, P.-W.; Lian, I.; Lo, Y.-H. Protein—ligand interaction detection with a novel method of transient induced molecular electronic spectroscopy (TIMES): experimental and theoretical studies. *ACS Cent. Sci.* **2016**, 2, 834–842.

- (24) Zheng, S.; Sajib, M. S. J.; Wei, Y.; Wei, T. Discontinuous Molecular Dynamics Simulations of Biomolecule Interfacial Behavior: Study of Ovispirin-1 Adsorption on a Graphene Surface. *J. Chem. Theory Comput.* **2021**, *17*, 1874–1882.
- (25) Sajib, M. S. J.; Wei, Y.; Mishra, A.; Zhang, L.; Nomura, K.-I.; Kalia, R. K.; Vashishta, P.; Nakano, A.; Murad, S.; Wei, T. Atomistic Simulations of Biofouling and Molecular Transfer of a Cross-linked Aromatic Polyamide Membrane for Desalination. *Langmuir* **2020**, *36*, 7658–7668.
- (26) Samieegohar, M.; Sha, F.; Clayborne, A. Z.; Wei, T. ReaxFF MD Simulations of Peptide-Grafted Gold Nanoparticles. *Langmuir* **2019**, *35*, 5029–5036.
- (27) Zheng, J.; Li, L.; Chen, S.; Jiang, S. Molecular simulation study of water interactions with oligo (ethylene glycol)-terminated alkanethiol self-assembled monolayers. *Langmuir* **2004**, *20*, 8931–8938
- (28) Chen, H.; Zhang, M.; Yang, J.; Zhao, C.; Hu, R.; Chen, Q.; Chang, Y.; Zheng, J. Synthesis and characterization of antifouling poly (N-acryloylaminoethoxyethanol) with ultralow protein adsorption and cell attachment. *Langmuir* **2014**, *30*, 10398–10409.
- (29) Sajib, M. S. J.; Sarker, P.; Wei, Y.; Tao, X.; Wei, T. Protein corona on gold nanoparticles studied with coarse-grained simulations. *Langmuir* **2020**, *36*, 13356–13363.
- (30) Guo, W.; Zou, X.; Jiang, H.; Koebke, K. J.; Hoarau, M.; Crisci, R.; Lu, T.; Wei, T.; Marsh, E. N. G.; Chen, Z. Molecular Structure of the Surface-Immobilized Super Uranyl Binding Protein. *J. Phys. Chem. B* **2021**, *125*, 7706–7716.
- (31) Yu, G.; Zhou, J. Understanding the curvature effect of silica nanoparticles on lysozyme adsorption orientation and conformation: a mesoscopic coarse-grained simulation study. *Phys. Chem. Chem. Phys.* **2016**, *18*, 23500–23507.
- (32) Käkinen, A.; Ding, F.; Chen, P.; Mortimer, M.; Kahru, A.; Ke, P. C. Interaction of firefly luciferase and silver nanoparticles and its impact on enzyme activity. *Nanotechnology* **2013**, *24*, No. 345101.
- (33) Tavakol, M.; Montazeri, A.; Naghdabadi, R.; Hajipour, M. J.; Zanganeh, S.; Caracciolo, G.; Mahmoudi, M. Disease-related metabolites affect protein—nanoparticle interactions. *Nanoscale* **2018**, *10*, 7108—7115.
- (34) Ramezani, F.; Rafii-Tabar, H. An in-depth view of human serum albumin corona on gold nanoparticles. *Mol. BioSyst.* **2015**, *11*, 454–462.
- (35) Quan, X.; Peng, C.; Zhao, D.; Li, L.; Fan, J.; Zhou, J. Molecular understanding of the penetration of functionalized gold nanoparticles into asymmetric membranes. *Langmuir* **2017**, 33, 361–371.
- (36) Osman, M. A.; Keller, B. A. Wettability of native silver surfaces. *Appl. Surf. Sci.* **1996**, *99*, 261–263.
- (37) Schrader, M. E. Ultrahigh vacuum techniques in the measurement of contact angles. III. Water on copper and silver. *J. Phys. Chem.* **1974**, *78*, 87–89.
- (38) Drelich, J.; Chibowski, E.; Meng, D. D.; Terpilowski, K. Hydrophilic and superhydrophilic surfaces and materials. *Soft Matter* **2011**, *7*, 9804–9828.
- (39) Sawai, M. V.; Waring, A. J.; Kearney, W. R.; McCray, P. B., Jr.; Forsyth, W. R.; Lehrer, R. I.; Tack, B. F. Impact of single-residue mutations on the structure and function of ovispirin/novispirin antimicrobial peptides. *Protein Eng.* **2002**, *15*, 225–232.
- (40) Souza, P. C.; Alessandri, R.; Barnoud, J.; Thallmair, S.; Faustino, I.; Grünewald, F.; Patmanidis, I.; Abdizadeh, H.; Bruininks, B. M.; Wassenaar, T. A.; Kroon, P. C.; Melcr, J.; Nieto, V.; Corradi, V.; Khan, H. M.; Domański, J.; Javanainen, M.; Martinez-Seara, H.; Reuter, N.; Best, R. B.; Vattulainen, I.; Monticelli, L.; Periole, X.; Tieleman, D. P.; de Vries, A. H.; Marrink, S. J. Martini 3: a general purpose force field for coarse-grained molecular dynamics. *Nat. Methods* **2021**, *18*, 382–388.
- (41) Abraham, M. J.; Murtola, T.; Schulz, R.; Páll, S.; Smith, J. C.; Hess, B.; Lindahl, E. GROMACS: High performance molecular simulations through multi-level parallelism from laptops to supercomputers. *SoftwareX* **2015**, *1-2*, 19–25.

- (42) Hu, G.; Jiao, B.; Shi, X.; Valle, R. P.; Fan, Q.; Zuo, Y. Y. Physicochemical properties of nanoparticles regulate translocation across pulmonary surfactant monolayer and formation of lipoprotein corona. *ACS Nano* **2013**, *7*, 10525–10533.
- (43) Hu, Q.; Bai, X.; Hu, G.; Zuo, Y. Y. Unveiling the molecular structure of pulmonary surfactant corona on nanoparticles. *ACS Nano* **2017**, *11*, 6832–6842.
- (44) Huang, J.; MacKerell, A. D., Jr. CHARMM36 all-atom additive protein force field: Validation based on comparison to NMR data. *J. Comput. Chem.* **2013**, *34*, 2135–2145.
- (45) Heinz, H.; Vaia, R. A.; Farmer, B. L.; Naik, R. R. Accurate simulation of surfaces and interfaces of face-centered cubic metals using 12–6 and 9–6 Lennard-Jones potentials. *J. Phys. Chem. C* **2008**, 112, 17281–17290.
- (46) Penna, M. J.; Mijajlovic, M.; Biggs, M. J. Molecular-level understanding of protein adsorption at the interface between water and a strongly interacting uncharged solid surface. *J. Am. Chem. Soc.* **2014**, *136*, 5323–5331.
- (47) McLoughlin, S. Y.; Kastantin, M.; Schwartz, D. K.; Kaar, J. L. Single-molecule resolution of protein structure and interfacial dynamics on biomaterial surfaces. *Proc. Natl. Acad. Sci. U.S.A.* **2013**, *110*, 19396–19401.
- (48) Kastantin, M.; Langdon, B. B.; Chang, E. L.; Schwartz, D. K. Single-molecule resolution of interfacial fibrinogen behavior: Effects of oligomer populations and surface chemistry. *J. Am. Chem. Soc.* **2011**, *133*, 4975–4983.
- (49) Samieegohar, M.; Ma, H.; Sha, F.; Jahan Sajib, M. S.; Guerrero-García, G. I.; Wei, T. Understanding the interfacial behavior of lysozyme on Au (111) surfaces with multiscale simulations. *Appl. Phys. Lett.* **2017**, *110*, No. 073703.
- (50) Vilaseca, P.; Dawson, K. A.; Franzese, G. Understanding and modulating the competitive surface-adsorption of proteins through coarse-grained molecular dynamics simulations. *Soft Matter* **2013**, *9*, 6978–6985.
- (51) Kabsch, W.; Sander, C. Dictionary of protein secondary structure: pattern recognition of hydrogen-bonded and geometrical features. *Biopolymers* **1983**, *22*, 2577–2637.

□ Recommended by ACS

From Protein Corona to Colloidal Self-Assembly: The Importance of Protein Size in Protein-Nanoparticle Interactions

Laurent Marichal, Serge Pin, et al.

JUNE 25, 2020

LANGMUIR

READ 🗹

Protein Nanoparticle Charge and Hydrophobicity Govern Protein Corona and Macrophage Uptake

Samantha M. Pustulka, Julie A. Champion, et al.

OCTOBER 15, 2020

ACS APPLIED MATERIALS & INTERFACES

READ 🗹

Size Dependence Unveiling the Adsorption Interaction of High-Density Lipoprotein Particles with PEGylated Gold Nanoparticles in Biomolecular Corona Formation

Gwi Ju Jang, Sang Yun Han, et al.

AUGUST 04, 2021

LANGMUIR

READ 🗹

An Analysis of the Binding Function and Structural Organization of the Protein Corona

Yuwei Zhang, Warren C. W. Chan, et al.

APRIL 15, 2020

JOURNAL OF THE AMERICAN CHEMICAL SOCIETY

READ 🗹

Get More Suggestions >